Photocatalytic Degradation of Tetrachloroethylene in Gas Phase on TiO_2 Films: A Kinetic Study

Gustavo E. Imoberdorf, Horacio A. Irazoqui, Alberto E. Cassano, and Orlando M. Alfano*

INTEC, Instituto de Desarrollo Tecnológico para la Industria Química, (Universidad Nacional del Litoral and CONICET), Güemes 3450, (3000) Santa Fe, Argentina

In this work, the degradation of tetrachloroethylene or perchloroethylene (PCE) in an air stream was studied for different values of PCE feed concentrations, relative humidity levels, and light intensities. The TiO_2 photocatalyst was deposited as a thin film on a borosilicate glass plate by means of a sol−gel technique. The reactor was operated under kinetic control regime. An expression of the intrinsic reaction kinetics was developed. This expression is based on a model of the absorption of radiant energy on the surface of the catalyst, followed by a detailed reaction mechanism based on a reaction scheme that involves $Cl^{\bullet}$ as an active reaction intermediate. Experimental results from a differential photoreactor were used to validate the proposed kinetic model and to determine the kinetic parameters by nonlinear regression of experimental data. The obtained results show: (1) first-order kinetics with respect to the PCE concentration, (2) linear dependence with the photon absorption rate, and (3) site-competitive adsorption between PCE and water, resulting in a dependence of the kinetics on the relative humidity.

Introduction

Several volatile organic chlorinated compounds such as tetrachloroethylene (perchloroethylene, PCE) are used as solvents at industrial scale in dry cleaning and metal degreasing facilities as well as in plastic manufacturing and fumigation. On one hand, these solvents are noninflammable and chemically stable and have excellent washing properties, but on the other, these compounds are toxic, carcinogenic, and extremely persistent in the environment. One interesting destructive, technological alternative for treating this type of pollutants is photocatalysis, a particular form of advanced oxidation processes that uses near-UV radiation and a solid semiconductor such as titanium dioxide.

The vast majority of the studies performed on the photocatalytic degradation of chlorinated ethylenes in the gas phase have been made employing trichloroethylene (TCE) as a model substrate. On the contrary, only few contributions on PCE oxidation can be found employing the same process. This is one of the reasons why most of the reaction paths or mechanisms proposed for PCE photocatalytic oxidation have been adapted from previous work on TCE.

Al-Ekabi et al.[1] published one of the few reports on PCE degradation. They performed experimental research on the photocatalytic oxidation of PCE and TCE with different concentrations of the pollutant, using titanium dioxide supported on a glass fiber mesh as the catalyst. The mesh was placed surrounding the UV lamp tube, giving rise to an annular reaction space. This article was properly complemented by that of Fukami et al.,[2] in which they were able to identify most of the intermediate and final products of the degradation reaction and proposed a plausible reaction path; in their work they used a batch reactor with the titanium dioxide catalyst supported on a borosilicate glass. Yamasaki et al.[3] studied the degradation of PCE in an air stream using a continuous, tubular, fixed bed reactor. They found that water vapor (air humidity) competes with PCE for the same catalyst active sites and that the reaction mechanism seems to be the same as the one they proposed for TCE photooxidation. Immediately after, Yamasaki and Araki[4] studied the degradation of TCE and PCE in a fixed bed reactor using TiO_2 pellets prepared by a sol−gel technique. They succeeded in making a detailed analysis of the reaction products from TCE and PCE and proposed a reaction mechanism in which the participation of an atomic chlorine radical intermediate species explains most of the observed results.

Despite being a different chemical compound, it is particularly important for this work to know the related studies performed with TCE because the photocatalytic reaction behavior seems to be very similar. Not all the published work is coincident with what the proposed reaction path is concerned. In some cases these discrepancies also extend to the detected reaction intermediate species and final products. One may cite the contributions of Anderson et al.,[5] Luo and Ollis,[6] Kim et al.,[7] Li and An,[8] Zhao et al.,[9] and Wang et al.[10] In some contributions the effect of water vapor on the reaction rate was additionally analyzed.[11−13] Some of these studies proposed a reaction kinetic equation based on the Langmuir−Hinshelwood−Hougen−Watson mechanism and on the basis of the model that best represents the observed results proceeded to estimate the unknown parameters. This type of approach can be found in the work reported by Dibble and Raupp,[11] Wang et al.,[14] Kim and Hong,[15] and Yamazaki-Nishida et al.[16]

The present work aims at obtaining the intrinsic kinetics of the PCE photocatalytic degradation reaction on a titanium dioxide film supported on a glass plate. For this purpose, a differential reactor has been specifically designed, with a particular configuration conceived to avoid transport phenomena interference on the

* To whom correspondence should be addressed. Tel.: +54-342-455 9175. Fax: +54-342-455 9185. E-mail: alfano@intec.unl.edu.ar.

10.1021/ie049185z CCC: $30.25
Published on Web 02/22/2005

reaction kinetics. As a consequence of this, the reactor configuration may be very different from those we might propose in the future for practical applications. If the obtained kinetic expression were actually an intrinsic one, it should be independent of the chosen reactor geometry. In the differential reactor, the inlet air stream containing PCE and controlled humidity was brought into contact with the catalyst films deposited on both sides of a flat borosilicate glass plate. The catalyst has been deposited using a sol−gel technique. The composite of the two catalytic films and the glass support was irradiated from both sides by means of two sets of seven lamps each (black light type) that have a small UV energy output. The irradiation reaching every point on each side of the plate was precisely computed on the basis of a radiation field model and experimentally validated. The gaseous stream circulates in the reaction cavity and is always in contact with the two catalytic films deposited on the glass plate. This arrangement permitted the variation of operating conditions in a wide range of the operating variables in such a way that it was possible to remove any form of external mass transfer resistance in the reacting system. Therefore, it was possible to work under conditions corresponding to the kinetic control regime. Under these conditions, it was possible to obtain intrinsic kinetic data.

The kinetic model was adapted from a mechanistic sequence based on work previously done to characterize the chemistry of the reaction, and with the experimental information obtained in the differential flat plate reactor, the reaction parameters could be regressed using a nonlinear multiparameter estimator. In deriving the kinetic expression for PCE degradation, it is assumed that the contribution to the reaction rate due to the propagation sequence involving atomic chlorine radicals ($Cl^{\bullet}$) is much more important than the direct action of the hydroxyl radicals ($OH^{\bullet}$) generated by the reaction step between the holes (h^+) and the (OH^-) ions adsorbed on the catalytic surface.[9,13] With the radiation field model, the local superficial rate of photon absorption (LSRPA) by the catalytic film was accurately predicted. This allowed us to calculate the terms in the final intrinsic kinetic expression that depend on the radiation field, before proceeding to the regression of those parameters related to the initiation step and the concentration-dependent, remaining part of the final expression. This procedure prevents the fact that uncertainties associated with the radiation field propagate to the true kinetic parameters. It is important to note that this independent calculation of the radiation field allowed us to reproduce the two limiting cases reported in the literature,[17] namely, (i) square root dependence with the photon absorption rate (when the incoming radiation flux is high) and (ii) linear dependence with the photon absorption rate (when the incident photon flux on the reactor window is low). The model of the LSRPA on the catalytic film is based on a three-dimensional light source with superficial emission model[18] for each one of the lamps used in the experimental device as well as a detailed consideration of the radiation attenuations caused by the different media encountered by the radiation beams as they travel between the lamps and the reaction plate (acrylic windows, borosilicate glass, and titanium dioxide film).

Experimental Section

Installation Description. The experiments were performed in the photocatalytic reactor sketched in Figure 1a. The reaction chamber was confined between two rectangular acrylic windows (19 × 9 cm^2), which is transparent in the useful wavelength range of UV radiation. At half distance between them, a rectangular plate of borosilicate glass (9 × 9 cm^2) covered with a thin layer of TiO_2 on its two sides was placed. The thin layers of TiO_2 were deposited using a sol−gel technique.[16] This catalytic plate was exposed to the radiation coming from two sets of seven UV-emitting lamps (Philips TL 4W/08 F4T5/BLB); each set faced one plate side. The lamps in each set were arranged with a separation between axes of 2.6 cm, and the distance from them to the reactor center plane was 4.3 cm. The borders of the catalytic plate (2.25 cm) were covered with an opaque film to achieve a homogeneous irradiation over the film area exposed to radiation (9 × 4.5 cm^2), as shown in Figure 1a. As a consequence of this, the photocatalytic reaction takes place only on the irradiated surface. The gaseous mixture flows through the rectangular opening between the plate and the acrylic windows of 2-mm width. The gas was fed from the bottom of the reactor, first passing through a flow distributor that consisted of a regularly perforated acrylic plate. The irradiation level on the catalytic film can be modified by means of specially designed optical filters.[19] Radiation fluxes were measured with a UV radiometer (International Light IL 1700 SED005/WBS320/W).

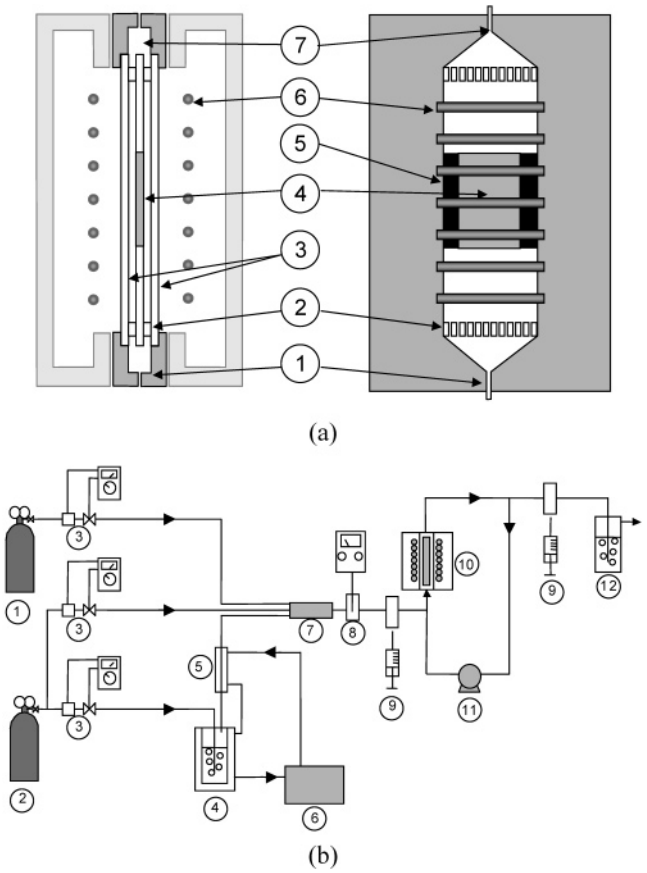

Figure 1. (a) Details of the photocatalytic reactor: (1) gas inlet, (2) flow homogenizer, (3) acrylic windows, (4) photocatalytic plate, (5) opaque film, (6) UV lamps, and (7) gas outlet. (b) Flowsheet of the experimental device: (1) PCE + air, (2) air, (3) mass flowmeter, (4) air humidifier, (5) heat exchanger, (6) thermostatic bath, (7) mixer, (8) thermohygrometer, (9) sampling device, (10) photoreactor, (11) recycle pump, and (12) gas scrubber.

Table 1. Experimental Operating Conditions

operating conditions	value
feed flow rate	20−200 $cm^3\ min^{-1}$
recirculating flow rate	2000 $cm^3\ min^{-1}$
temperature	20 °C
pressure	1 atm
inlet PCE concentration	10−30 mg m^{-3}
relative humidity	10−100%
reactive surface	81 cm^2
irradiation level	24−100%

In Figure 1b, the experimental setup is schematically shown. A recycle loop that consists of the photoreactor and the circulation pump allowed us to operate the reactor as a differential one. The recycle was fed with a mixture of three streams consisting of air, water-saturated air, and a PCE−air mixture, respectively. Prescribed ratios between the mass flows of these streams allowed us to obtain a controlled mass flow, as well as the desired PCE concentration and humidity. The used air was of chromatographic quality (Air Liquide). The PCE−air mixture was prepared from the same quality air and liquid PCE (Merck, p.a. quality). The water-saturated air stream was obtained by bubbling the air stream through glass saturation flask containing distillated water at 20 °C. The flow rates of the three streams were controlled with online mass-flow controllers (Matheson Corp.). The temperature and the humidity of the feed stream were measured with an online thermohygrometer (Oakton 35612-00) located before the inlet point of the recycling system.

Catalyst Preparation. Except for some modifications, the technique proposed by Yamazaki-Nishida et al.[16] was used to fix the titanium dioxide on the supporting plate. A volume of 415 cm^3 of triple-distilled water was mixed with 4.5 cm^3 of concentrated nitric acid (Anedra, 65%). Then, 35 cm^3 of titanium isopropoxide (Aldrich, 97%) solution was added to this mixture and peptized under stirring during 10 h at 80 °C until a clear sol was obtained. After cooling, 0.01% of a surfactant was added to promote a uniform spreading of the titanium dioxide on the carefully cleaned supporting plates. These plates were washed with isopropyl alcohol and triple-distilled water for 20 min under sonication. Then they were calcined for 8 h at 500 °C to remove any trace of organic materials that might still remain on the surface. The films were deposited by dip-coating of the glass plates in the liquid mixture at a withdrawal speed of 3 cm min^{-1} at ambient temperature (25 °C). The plates were dried in an oven at 80 °C and then calcined at 200 °C for 6 h.

The amount of titanium dioxide deposited was measured by a titration procedure[20] that involves the spectrophotometric determination of the peroxotitanate formed from titanium sulfate and hydrogen peroxide. The average superficial weight of TiO_2 on the covered glass was 0.023 mg cm^{-2}. From XRD measurements it was concluded that all the immobilized TiO_2 was in the Anatase crystalline form.

Experimental Procedures. Experiments were performed with different PCE concentrations, humidity, air flow rates, and irradiation levels (Table 1). The temperature and pressure in all experiments were 20 °C and 1 atm, respectively. Before each experiment, the operating variables were fixed in the pre-established values and the lamps were switched on. Measurements were taken after 3 h to ensure a steady-state operation of the reaction system and constant light intensity. The PCE concentrations in the inlet and outlet streams were determined by offline gas chromatography (Hewlett-Packard 5890; J&W1257032 column; FID detector). The outlet stream was also analyzed by gas chromatography−mass spectroscopy techniques (Shimadzu QP-5000) for detecting any possible stable intermediate species and/or reaction byproducts.

The spectral radiation absorption of the photocatalytic plate, acrylic windows, and filters was measured with a UV−vis spectrophotometer (Varian Cary, 100 Bio) as a function of the wavelength within the emission range of the lamps (from 310 to 410 nm).

Reaction Scheme and Kinetic Model

The reactor operates in steady state. The recirculation flow rate (2000 cm^3/min) is large enough to lower diffusive resistances to negligible levels, also allowing to operate the photoreactor as a differential one under kinetic control regime.

From the mass balance for the recycle (including photoreactor and pump), it is possible to obtain the PCE reaction rate from the measurable variables:

$$\langle r_{PCE}\rangle_{Ar} = \frac{Q^{in}(\langle C_{PCE}\rangle^{out} - \langle C_{PCE}\rangle^{in})}{Ar} \qquad (1)$$

where Q^{in} is the volumetric flow rate of the stream fed to the loop, $\langle C_{PCE}\rangle^{in}$ and $\langle C_{PCE}\rangle^{out}$ are the averaged PCE concentrations of the inlet and outlet streams of the loop, respectively, and Ar is the reaction area of the photocatalytic plate. Thus, eq 1 allows us to obtain the experimental reaction rates under different operating conditions.

It should be noted that it is beyond the scope of this work to postulate a reaction mechanism. Instead, we looked for a plausible reaction scheme proposed by other researchers for systems showing many features in common with ours, as it is the case of the mineralization reaction of TCE. We require the adopted reaction mechanism to be consistent with the observed features of the degradation kinetics while keeping enough simplicity to be useful for practical applications and, specifically, for the design of a bench-scale reactor where other phenomena are irreducibly coupled with chemical kinetics. With the simplifications valid for our range of experimental conditions, the adopted mechanism will offer us a sound kinetic expression showing the parameters to be regressed from experiments.

An expression of the intrinsic reaction kinetics was developed on the basis of the reaction scheme summarized in Table 2. It is based on the mechanism proposed by Sanhueza et al.[21] for TCE degradation in the gas phase. Although it is not fully agreed upon, this reaction scheme was accepted by many authors.[6,8,9,13,22] Yamazaki and Araki[4] developed a similar mechanism for the PCE reaction. On the basis of these studies, the current reaction scheme was proposed, where it is considered that the PCE degradation is produced mainly by the $Cl^{\bullet}$ radical attack. In subsequent reactions, this radical is regenerated, producing a chain propagation mechanism.

The reaction begins with the generation of electron−hole pairs on the irradiated TiO_2 surface. To prevent the recombination of the charge carriers, the electrons and holes have to be trapped. The holes may react with adsorbed water and superficial OH^- ions to generate

Table 2. Reaction Mechanism

process	reaction steps	reaction rates
initiation:	$TiO_2 \rightarrow TiO_2 + e^- + h^+$	r_g
	$h^+ + H_2O_{ads} \rightarrow OH^\bullet + H^+$ }	$k_1[H_2O]_{ads}[h^+]$
	$h^+ + HO^-_{ads} \rightarrow OH^\bullet$ }	
	$e^- + O_2 \rightarrow O_2^{\bullet -}$	$k_2[O_2][e^-]$
($Cl^\bullet$) generation:	$C_2Cl_{4\ ads} + OH^\bullet \rightarrow C_2Cl_4OH^\bullet$	$k_3[C_2Cl_4]_{ads}[OH^\bullet]$
	$C_2Cl_4OH^\bullet + O_2 \rightarrow C_2Cl_4OHOO^\bullet$	$k_4[C_2Cl_4OH^\bullet][O_2]$
	$2\ C_2Cl_4OHOO^\bullet \rightarrow 2\ C_2Cl_4OHO^\bullet + O_2$	$k_5[C_2Cl_4OHOO^\bullet]^2$
	$C_2Cl_4OHO^\bullet \rightarrow C_2Cl_3OHO + Cl^\bullet$	$k_6[C_2Cl_4OHO^\bullet]$
chain propagation:	$C_2Cl_{4\ ads} + Cl^\bullet \rightarrow C_2Cl_5^\bullet$	$k_7[C_2Cl_4]_{ads}[Cl^\bullet]$
	$C_2Cl_5^\bullet + O_2 \rightarrow C_2Cl_5OO^\bullet$	$k_8[C_2Cl_5^\bullet][O_2]$
	$2\ C_2Cl_5OO^\bullet \rightarrow 2\ C_2Cl_5O^\bullet + O_2$	$k_9[C_2Cl_5OO^\bullet]^2$
	$C_2Cl_5O^\bullet \rightarrow CCl_2O + CCl_3^\bullet$	$k_{10}[C_2Cl_5O^\bullet]$
	$C_2Cl_5O^\bullet \rightarrow C_2Cl_4O + Cl^\bullet$	$k_{11}[C_2Cl_5O^\bullet]$
	$CCl_3^\bullet + O_2 \rightarrow CCl_3OO^\bullet$	$k_{12}[CCl_3^\bullet][O_2]$
	$2\ CCl_3OO^\bullet \rightarrow 2\ CCl_3O^\bullet + O_2$	$k_{13}[CCl_3OO^\bullet]^2$
	$CCl_3O^\bullet \rightarrow CCl_2O + Cl^\bullet$	$k_{14}[CCl_3O^\bullet]$
ending reactions:	$e^- + h^+ \rightarrow$ heat	$k_{15}[h^+][e^-]$
	$Cl^\bullet + M \rightarrow$ products	$k_{16}[Cl^\bullet][M]$
nonradical reaction:	$CCl_2O + H_2O \rightarrow CO_2 + 2\ HCl$	
adsorption:	$C_2Cl_4 + \text{sites} \leftrightarrow C_2Cl_{4\ ads}$	thermodynamic equilibrium
	$H_2O + \text{sites} \leftrightarrow H_2O_{ads}$	thermodynamic equilibrium

$OH^\bullet$ radicals, and the electrons can be trapped by gaseous oxygen generating superoxide radicals ($O_2^{\bullet -}$). The presence of oxygen on the surface is very important to prevent the reduction of the Ti^{4+} to Ti^{3+} and, consequently, a drastic decrease of the reaction rate. The electrons and holes that are not trapped will recombine, and energy will be lost as heat.

The PCE degradation reaction is produced by two parallel steps: (i) reaction attack by $OH^\bullet$ radicals and (ii) chain reaction attack by $Cl^\bullet$ radicals. Although in this scheme the main chemically active species for PCE degradation are the $Cl^\bullet$ radicals, the attack of the $OH^\bullet$ radicals to PCE is a necessary step to generate the $Cl^\bullet$ radicals.

The $Cl^\bullet$ radical combines with the double bond of the adsorbed PCE molecule. Then, the formed radical reacts with oxygen to form a peroxyl radical, which reacts with another peroxyl radical to give an alkoxyl radical. This reaction intermediate can react to form phosgene and a trichloromethyl radical or, alternatively, release a $Cl^\bullet$ radical to form C_2Cl_4O. The trichloromethyl radical reacts through a similar path to finally form phosgene and regenerate the $Cl^\bullet$ radical in a propagation sequence. Phosgene reacts with water vapor to form CO_2 and HCl. This reaction scheme ends up with the complete mineralization of PCE.

The formation of carbon tetrachloride (as one possible termination reaction) was not incorporated into this model because this compound was not observed as a byproduct. As a result of the very high reactivity of the $Cl^\bullet$ radical, it is possible to propose several other termination reactions. To simplify the kinetic expression, in our model we have grouped them in a single reaction:[23] $Cl^\bullet + M \rightarrow$ Products, where M may be water, other radicals, the reactor walls, or other surfaces in the recycle loop. To complete this description it is worthy to note that the reaction between $Cl^\bullet$ and water is described by several authors[8,13] as one of the main inhibition effects for $Cl^\bullet$ radicals in the chain reaction. As a result of the additional difficulty to distinguish between adsorbed radicals and free radicals very near to the photocatalyst surface, the adsorption of free radicals is not indicated in the elementary steps proposed in Table 2. Consequently, we have not explicitly balanced sites in each step to derive our kinetic model.

On the basis of the adopted mechanism, the PCE degradation rate is

$$r_{PCE} = -k_3[PCE]_{ads}[OH^\bullet] - k_7[PCE]_{ads}[Cl^\bullet] \quad (2)$$

Assuming that the PCE elimination through the first step of the chain propagation mechanism is the most important when compared with that involving the direct hydroxyl attack,[9,13] it is possible to neglect the first term of eq 2, to obtain:

$$r_{PCE} = -k_7[PCE]_{ads}[Cl^\bullet] \quad (3)$$

The steady-state approximation may be applied to the net generation rates of free radicals $OH^\bullet$, $Cl^\bullet$, "free" electrons (e^-), and holes (h^+):

$$r_{OH^\bullet} = k_1[H_2O]_{ads}[h^+] - k_3[PCE]_{ads}[OH^\bullet] = 0 \quad (4)$$

$$r_{h^+} = r_g - k_{15}[e^-][h^+] - k_1[H_2O]_{ads}[h^+] = 0 \quad (5)$$

$$r_{e^-} = r_g - k_{15}[e^-][h^+] - k_2[O_2][e^-] = 0 \quad (6)$$

where $r_{OH^\bullet}$, r_{h^+}, and r_{e^-} are the reaction rates of $OH^\bullet$, holes, and electrons, respectively, and r_g is the electron−hole rate generation that is related to the UV irradiation of the catalytic surface. From eq 4 we obtain

$$[OH^\bullet] = \frac{k_1[H_2O]_{ads}}{k_3[PCE]_{ads}}[h^+] \quad (7)$$

and from eqs 5 and 6, the following expression for the concentration of holes can be derived:

$$[h^+] = \sqrt{\left(\frac{k_2[O_2]}{2k_{15}}\right)^2 + \frac{k_2[O_2]}{k_{15}k_1[H_2O]_{ads}}r_g} - \frac{k_2[O_2]}{2k_{15}} \quad (8)$$

The steady-state approximation may be applied to the net generation rates of free radicals participating in the chain propagation and $Cl^\bullet$ generation, to obtain

$$[Cl^\bullet] = \frac{k_3[PCE]_{ads}[OH^\bullet]}{k_{16}[M]} \quad (9)$$

With these approximations, the overall rate of PCE elimination in terms of surface concentrations is

$$r_{PCE} = -\frac{k_1 k_2 k_7 [PCE]_{ads} [H_2O]_{ads} [O_2]}{2k_{15} k_{16} [M]} \left(-1 + \sqrt{1 + \frac{4k_{15}}{k_1 k_2 [H_2O]_{ads} [O_2]} r_g} \right) \quad (10)$$

The surface concentrations of adsorbed PCE and water can be obtained from a balance of active sites, assuming that there are no mass transfer limitations and taking into account that PCE and water compete for the same adsorption sites, as has been reported by previously quoted authors. Consequently, surface concentrations can be related to gas-phase concentrations by means of the following expressions:

$$[PCE]_{ads} = \frac{K_{PCE} [Sites] [PCE]_{gas}}{(1 + K_{PCE} [PCE]_{gas} + K_W [H_2O]_{gas})} \quad (11)$$

$$[H_2O]_{ads} = \frac{K_W [Sites] [H_2O]_{gas}}{(1 + K_{PCE} [PCE]_{gas} + K_W [H_2O]_{gas})} \quad (12)$$

where K_{PCE} and K_W are the adsorption equilibrium constants of PCE and water, respectively, and [Sites] is the surface concentration of sites available for adsorption on the TiO_2 catalyst film. Substituting eqs 11 and 12 into eq 10:

$$r_{PCE} = -\frac{k_1 k_2 k_7 K_{PCE} K_W [Sites]^2 [PCE]_{gas} [H_2O]_{gas} [O_2]}{2k_{15} k_{16} [M] (1 + K_{PCE} [PCE]_{gas} + K_W [H_2O]_{gas})^2} \times \left(-1 + \sqrt{1 + \frac{4k_{15} (1 + K_{PCE} [PCE]_{gas} + K_W [H_2O]_{gas})}{k_1 k_2 K_W [Sites] [O_2] [H_2O]_{gas}} r_g} \right) \quad (13)$$

With the definitions

$$\alpha_1 = \frac{k_1 k_2 k_7 K_{PCE} K_W [Sites]^2 [O_2]}{2k_{15} k_{16} [M]} \quad (14)$$

$$\alpha_2 = \frac{4k_{15}}{k_1 k_2 K_W [Sites] [O_2]} \quad (15)$$

Equation 13 can be simplified into the following expression:

$$r_{PCE} = -\frac{\alpha_1 [PCE]_{gas} [H_2O]_{gas}}{(1 + K_{PCE} [PCE]_{gas} + K_W [H_2O]_{gas})^2} \left(-1 + \sqrt{\frac{1 + K_{PCE} [PCE]_{gas} + K_W [H_2O]_{gas}}{[H_2O]_{gas}} \alpha_2 r_g(\underline{x}) + 1} \right) \quad (16)$$

The local superficial rate of electron−hole pair generation r_g is given by:

$$r_g(\underline{x}) = \int_{\lambda_1}^{\lambda_2} \Phi_\lambda e_\lambda^{a,s}(\underline{x})\, d\lambda \cong \sum_\lambda \Phi_\lambda e_\lambda^{a,s}(\underline{x}) \quad (17)$$

where Φ_λ is the spectral primary quantum yield and $e_\lambda^{a,s}$ is the spectral LSRPA. With the definition of a wavelength averaged primary quantum yield, $\bar{\Phi}$, eq 17 can be written:

$$r_g(\underline{x}) = \sum_\lambda \Phi e_\lambda^{a,s}(\underline{x}) = \bar{\Phi} \sum_\lambda e_\lambda^{a,s}(\underline{x}) = \bar{\Phi} e^{a,s}(\underline{x}) \quad (18)$$

Substitution of eq 18 in eq 16 gives:

$$r_{PCE} = -\frac{\alpha_1 [PCE]_{gas} [H_2O]_{gas}}{(1 + K_{PCE} [PCE]_{gas} + K_W [H_2O]_{gas})^2} \left(-1 + \sqrt{\frac{1 + K_{PCE} [PCE]_{gas} + K_W [H_2O]_{gas}}{[H_2O]_{gas}} \alpha_2 \bar{\Phi} e^{a,s}(\underline{x}) + 1} \right) \quad (19)$$

To evaluate eq 19 it is necessary to know the radiation field distribution and then to obtain $e^{a,s}(\underline{x})$ on the photocatalytic surface.

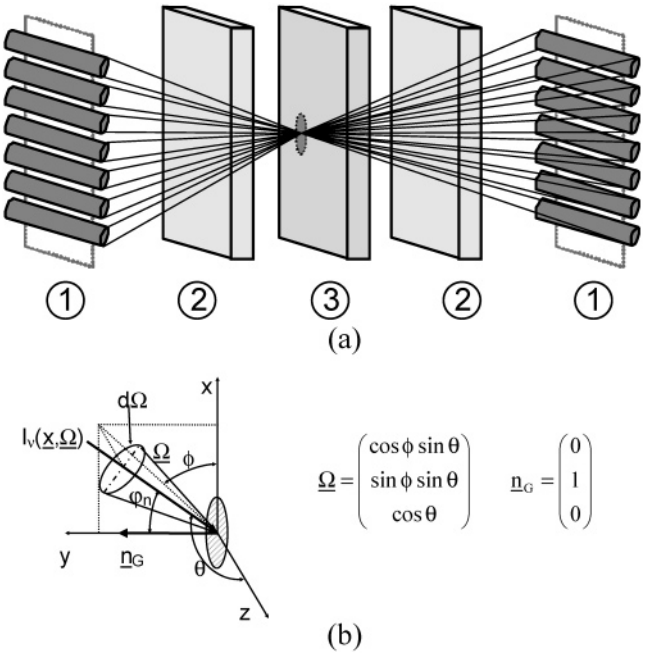

Figure 2. (a) Schematic representation of the emitting system: (1) black-light lamps, (2) acrylic windows, and (3) photocatalytic glass plate. (b) Coordinate system adopted for the reactor-lamps system.

Radiation Field Model

The LSRPA was evaluated at each point on the TiO_2 films, taking into account the radiation coming from each lamp on either side of the plate, as shown in Figure 2a. Although both the acrylic windows and the borosilicate glass plate used as support of the TiO_2 catalyst have satisfactory UV transmission properties in the range 310−410 nm, they attenuate the intensity of the UV radiation beams to some extent. This effect was also included in the model of the radiation field.

Our purpose here is to advance a first approach to the complexities of a beam attenuation when traversing a composite of TiO_2 layers deposited on both sides of a glass plate. As a radiation beam traverses the film, its intensity will change due to three different causes: (a) part of the energy it carries will be scattered into other directions (out-scattering), (b) the intensity of a

beam may be reinforced with the energy lost from other beams as scattered radiation (in-scattering), and (c) true energy absorption. We will assume that scattered radiation is a small fraction of the total radiation that any beam is carrying at any point in the thin film, and after being scattered this energy is quickly lost to the radiation field due to true absorption and transformed into other forms of energy. Therefore, true energy absorption remains as the main factor of beam attenuation through the catalytic film.

With these assumptions, the ray-tracing problem can be brought close to a problem of geometrical optics, while the energy attenuation of beams is reduced to an energy absorption problem in a composite medium.

The local net radiation flux on the catalytic film, q_λ, corresponding to a given wavelength λ, is:

$$q_\lambda(\underline{x}) = \underline{n}_G \cdot \underline{q}_\lambda(\underline{x}) = \int_{\Omega_L} I_\lambda(\underline{x},\underline{\Omega})\underline{\Omega}\cdot\underline{n}_G \, d\Omega \quad (20)$$

where $\underline{n}_G$ is the outwardly directed unit normal to the catalytic film and I_λ is the intensity associated to a beam of rays carrying energy of wavelength λ in the direction of the unit vector $\underline{\Omega}$. According to the coordinate system adopted (Figure 2b),

$$\underline{\Omega}\cdot\underline{n}_G = \cos\varphi_n = \sin\phi \sin\theta \quad (21)$$

and

$$d\Omega = \sin\theta \, d\theta \, d\phi \quad (22)$$

Replacing eqs 21 and 22 in eq 20:

$$q_\lambda(\underline{x}) = \int_{\phi_L}\int_{\theta_L} I_\lambda(\underline{x},\phi,\theta)\sin^2\theta \sin\phi \, d\theta \, d\phi \quad (23)$$

To solve this equation, we will make use of the three-dimensional source with superficial emission model[18] and the ray-tracing method.[24] In this model, the additive effect of each lamp on the local net radiation flux is taken into account. This means that the radiation flux was solved for each lamp independently, and then the contributions of all lamps were added up:

$$q_\lambda(\underline{x}) = \sum_{i=1}^{n}\int_{\phi_{L_i}}\int_{\theta_{L_i}} I_{\lambda,i}(\underline{x},\phi,\theta)\sin^2\theta \sin\phi \, d\theta \, d\phi \quad (24)$$

Note that the radiation intensity arriving from each lamp does not come from all directions, but only from those within the limits defined by the vision angle that relates each point of incidence with the dimensions and position of each lamp (see Appendix):

$$I_{\lambda,i}(\underline{x},\phi,\theta) = \begin{cases} 0 & (\phi,\theta) < (\phi_{min,i}, \theta_{min,i}) \\ I_{\lambda,L_i}(x,\phi,\theta) & (\phi_{min,i}, \theta_{min,i}) < (\phi,\theta) < (\phi_{max,i}, \theta_{max,i}) \\ 0 & (\phi_{max,i}, \theta_{max,i}) < (\phi, \theta) \end{cases} \quad (25)$$

Considering the assumptions made on the lamp emission model, the boundary condition results:[18]

$$I_{\lambda,L_i}(\underline{x},\phi,\theta) = I_{\lambda,L_i} = \frac{P_{\lambda\cdot L_i}}{2\pi^2 r_L z_L} \quad (26)$$

where $P_{\lambda\cdot L_i}$ is the spectral emission power of the lamp, and r_L and z_L are the radius and length of the lamp, respectively.

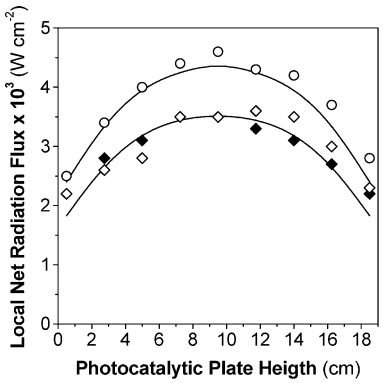

Figure 3. Experimental and predicted radiation fluxes. Experimental values at $z = 1.5$ cm (◇), $z = 4.5$ cm (○), and $z = 7.5$ cm (◆). Model predictions: solid lines.

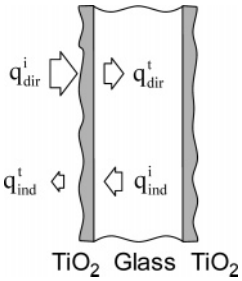

Figure 4. Schematic representation of direct and indirect radiation fluxes on the TiO_2 film.

At this point no participative medium was considered; it results from the fact that air, PCE, and water vapor do not absorb radiation in the wavelength range of the lamp emission. Substituting eqs 25 and 26 into eq 24:

$$q_\lambda(\underline{x}) = \sum_{i=1}^{n}\int_{\phi_{min,L_i}}^{\phi_{max,L_i}}\int_{\theta_{min,L_i}(\phi)}^{\theta_{max,L_i}(\phi)} I_{\lambda,L_i}\sin^2\theta \sin\phi \, d\theta \, d\phi \quad (27)$$

To solve eq 27 using the ray-tracing method,[24] the limiting angles corresponding to the irradiation visual angles from the surface of every lamp to every incident point on the catalytic surface were calculated. In this way, eq 27 after substitution of eq 26 was numerically solved.

To validate the proposed radiation model, radiation fluxes arriving at the catalytic surface were measured with a UV-radiometer. Figure 3 shows a comparison of the experimental data with predictions from the model.

At each point, the LSRPA was obtained as the sum of two radiation fluxes: $q_{dir,\lambda}$ and $q_{ind,\lambda}$, as is schematically shown in Figure 4.

$$e^{a,s}(\underline{x}) = [q^i_{dir}(\underline{x}) - q^t_{dir}(\underline{x})] + [q^i_{ind}(\underline{x}) - q^t_{ind}(\underline{x})] \quad (28)$$

where $q^i_{dir}(\underline{x})$ and $q^t_{dir}(\underline{x})$ are the incident and transmitted net radiation fluxes, given by eq 27. These fluxes result from the radiation emitted by the seven lamps facing the film considered and attenuated by the acrylic extinction and acrylic/TiO_2 extinction respectively:

$$q^{\mathrm{i}}_{\mathrm{dir}}(\underline{x}) = \sum_{\lambda=310\mathrm{nm}}^{410\mathrm{nm}} \sum_{i=1}^{7} \int_{\phi_{\min,\mathrm{L}_i}}^{\phi_{\max,\mathrm{L}_i}} \int_{\theta_{\min,\mathrm{L}_i}(\phi)}^{\theta_{\max,\mathrm{L}_i}(\phi)} I_{\lambda,\mathrm{L}_i} \exp\left(-\frac{\kappa_{\lambda,\mathrm{a}} e_{\mathrm{a}}}{\cos\theta_{\mathrm{n}}}\right) \sin^2\phi \, \mathrm{d}\theta \, \mathrm{d}\phi \quad (29)$$

$$q^{\mathrm{t}}_{\mathrm{dir}}(\underline{x}) = \sum_{\lambda=310\mathrm{nm}}^{410\mathrm{nm}} \sum_{i=1}^{7} \int_{\phi_{\min,\mathrm{L}_i}}^{\phi_{\max,\mathrm{L}_i}} \int_{\theta_{\min,\mathrm{L}_i}(\phi)}^{\theta_{\max,\mathrm{L}_i}(\phi)} I_{\lambda,\mathrm{L}_i} \exp\left(-\frac{\kappa_{\lambda,\mathrm{a}} e_{\mathrm{a}}}{\cos\theta_{\mathrm{n}}} - \frac{\kappa_{\lambda,\mathrm{f}} e_{\mathrm{f}}}{\cos\theta_{\mathrm{n}}}\right) \sin^2\phi \sin\theta \, \mathrm{d}\theta \, \mathrm{d}\phi \quad (30)$$

Similarly, $q^{\mathrm{i}}_{\mathrm{ind}}(\underline{x})$ and $q^{\mathrm{t}}_{\mathrm{ind}}(\underline{x})$ are the incident and transmitted net radiation fluxes, respectively, coming from the seven lamps located on the opposite side of the surface considered, in this case attenuated by acrylic/TiO_2/glass and acrylic/TiO_2/glass/TiO_2, successively:

$$q^{\mathrm{i}}_{\mathrm{ind}}(\underline{x}) = \sum_{\lambda=310\mathrm{nm}}^{410\mathrm{nm}} \sum_{i=8}^{14} \int_{\phi_{\min,\mathrm{L}_i}}^{\phi_{\max,\mathrm{L}_i}} \int_{\theta_{\min,\mathrm{L}_i}(\phi)}^{\theta_{\max,\mathrm{L}_i}(\phi)} I_{\lambda,\mathrm{L}_i} \exp\left(-\frac{\kappa_{\lambda,\mathrm{a}} e_{\mathrm{a}}}{\cos\theta_{\mathrm{n}}} - \frac{\kappa_{\lambda,\mathrm{f}} e_{\mathrm{f}}}{\cos\theta_{\mathrm{n}}} - \frac{\kappa_{\lambda,\mathrm{g}} e_{\mathrm{g}}}{\cos\theta_{\mathrm{n}}}\right) \sin^2\phi \sin\theta \, \mathrm{d}\theta \, \mathrm{d}\phi \quad (31)$$

$$q^{\mathrm{t}}_{\mathrm{ind}}(\underline{x}) = \sum_{\lambda=310\mathrm{nm}}^{410\mathrm{nm}} \sum_{i=8}^{14} \int_{\phi_{\min,\mathrm{L}_i}}^{\phi_{\max,\mathrm{L}_i}} \int_{\theta_{\min,\mathrm{L}_i}(\phi)}^{\theta_{\max,\mathrm{L}_i}(\phi)} I_{\lambda,\mathrm{L}_i} \exp\left(-\frac{\kappa_{\lambda,\mathrm{a}} e_{\mathrm{a}}}{\cos\theta_{\mathrm{n}}} - \frac{\kappa_{\lambda,\mathrm{g}} e_{\mathrm{g}}}{\cos\theta_{\mathrm{n}}} - \frac{2\kappa_{\lambda,\mathrm{f}} e_{\mathrm{f}}}{\cos\theta_{\mathrm{n}}}\right) \sin^2\phi \sin\theta \, \mathrm{d}\theta \, \mathrm{d}\phi \quad (32)$$

where $\kappa_{\lambda,\mathrm{a}}$, $\kappa_{\lambda,\mathrm{g}}$, and $\kappa_{\lambda,\mathrm{f}}$ are the spectral absorption coefficients of the acrylic, glass, and TiO_2 film, e_{f}, e_{a}, and e_{g} are the thickness of each media, and θ_{n} is the angle between the ray trajectory and the film outwardly directed normal.

The final expression of the LSRPA at each point on the catalytic plate is given by:

$$e^{\mathrm{a,s}}(\underline{x}) = \sum_{\lambda=310\mathrm{nm}}^{410\mathrm{nm}} \sum_{i=1}^{7} \int_{\phi_{\min,i}}^{\phi_{\max,i}} \int_{\theta_{\min,i}(\phi)}^{\theta_{\max,i}(\phi)} I_{\lambda,\mathrm{Lamp}_i} \exp\left(-\frac{\kappa_{\lambda,\mathrm{a}} e_{\mathrm{a}}}{\cos\theta_{\mathrm{n}}}\right) \left[1 - \exp\left(-\frac{\kappa_{\lambda,\mathrm{f}} e_{\mathrm{f}}}{\cos\theta_{\mathrm{n}}}\right)\right] \sin^2\phi \sin\theta \, \mathrm{d}\theta \, \mathrm{d}\phi + \sum_{\lambda=310\mathrm{nm}}^{410\mathrm{nm}} \sum_{i=8}^{14} \int_{\phi_{\min,i}}^{\phi_{\max,i}} \int_{\theta_{\min,i}(\phi)}^{\theta_{\max,i}(\phi)} I_{\lambda,\mathrm{Lamp}_i} \exp\left(-\frac{\kappa_{\lambda,\mathrm{a}} e_{\mathrm{a}}}{\cos\theta_{\mathrm{n}}} - \frac{\kappa_{\lambda,\mathrm{g}} e_{\mathrm{g}}}{\cos\theta_{\mathrm{n}}} - \frac{\kappa_{\lambda,\mathrm{f}} e_{\mathrm{f}}}{\cos\theta_{\mathrm{n}}}\right) \times \left[1 - \exp\left(-\frac{\kappa_{\lambda,\mathrm{f}} e_{\mathrm{f}}}{\cos\theta_{\mathrm{n}}}\right)\right] \sin^2\phi \sin\theta \, \mathrm{d}\theta \, \mathrm{d}\phi \quad (33)$$

Values of $\kappa_{\lambda,\mathrm{a}} e_{\mathrm{a}}$, $\kappa_{\lambda,\mathrm{f}} e_{\mathrm{f}}$, and $\kappa_{\lambda,\mathrm{g}} e_{\mathrm{g}}$ were determined from spectral transmittance measurements (Figure 5a). This equation was numerically solved for each UV filter used in the experimental runs (Figure 5b).

Figure 6 shows the resulting net radiation flux field at the photocatalytic surface. The inner rectangle represents the surface exposed to radiation where the reaction takes place. The difference between the maximum and minimum values of the radiation flux on the reactive zone is 9%, while for the whole window is 58%. The small difference in the radiation flux on the photocatalytic surface allows us to consider an average value of LSRPA for this kinetic study:

$$\langle e^{\mathrm{a,s}} \rangle_{\mathrm{Ar}} = \frac{\int_{\mathrm{Ar}} e^{\mathrm{a,s}}(\underline{x}) \, \mathrm{d}A}{\mathrm{Ar}} \quad (34)$$

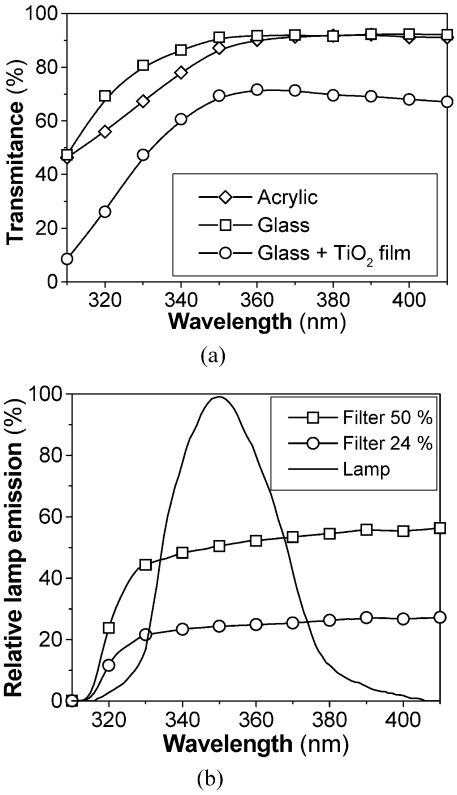

Figure 5. (a) Transmittance of glass, acrylic windows, and glass plate with TiO_2 film. (b) Lamp spectral emission and transmittance of optical filters.

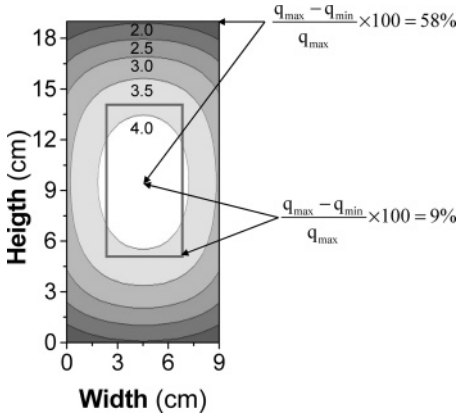

Figure 6. Contour graphic of the predicted radiation flux field. Key: (—) net radiation flux $q(\underline{x}) \times 10^3$ (W/cm^2).

Experimental Results

No reaction of PCE was observed in absence of either the TiO_2 photocatalyst or UV irradiation. The PCE degradation reaction was examined under several concentrations of reactants, humidity, and irradiation levels. Stable intermediates or byproducts were not detected by GC−MS. Therefore, under the studied conditions the mineralization of PCE was complete.

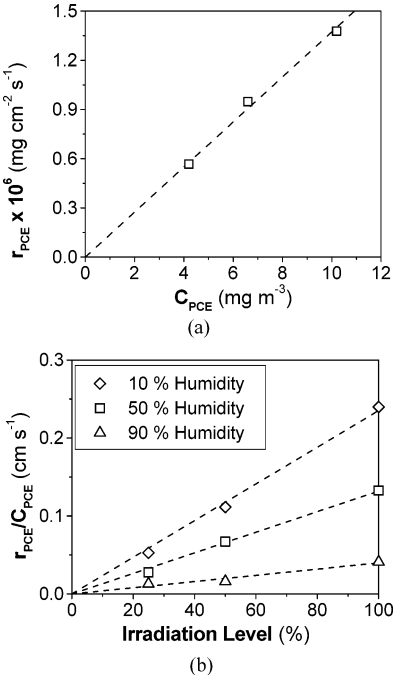

Figure 7. (a) PCE reaction rate as a function of PCE concentration. (b) PCE reaction rate divided by the PCE concentration vs the irradiation level. Key: (□) experimental values, (- - -) linear regression of experimental values.

The experimental results reported in Figure 7a show a linear dependence of the PCE reaction rate with respect to the PCE concentration in the gas phase. These results suggest that $K_{PCE}[PCE]_{gas} \ll 1 + K_W[H_2O]_{gas}$, and consequently, from eq 19 we conclude that the expression of the reaction rate can be simplified as follows:

$$r_{PCE} = -\frac{\alpha_1[PCE]_{gas}[H_2O]_{gas}}{(1+K_W[H_2O]_{gas})^2}\left(-1+\sqrt{\frac{1+K_W[H_2O]_{gas}}{[H_2O]_{gas}}\alpha_2\bar{\Phi}e^{a,s}+1}\right) \quad (35)$$

The effect of the irradiation level on the PCE reaction rate is shown in Figure 7b. The radiation flux on the glass plate was modified using specially designed filters[19] that where located between the reactor windows and the lamps (Figure 5b). The irradiation level was referred to the highest light intensity used, corresponding to the reactor without filters. Three humidity conditions (10, 50, and 90%) with three irradiation levels (24, 50, and 100%) were studied. A linear dependence of the PCE reaction rate with respect to the irradiation level was observed in all cases. These results clearly indicate that the reaction kinetic is not saturated with respect to the irradiation level. The same results were observed by Yamazaki et al.[3]

It should be noticed that, under low irradiation conditions, where $\{(1 + K_W[H_2O]_{gas})/[H_2O]_{gas}\}\alpha_2\bar{\Phi}e^{a,s} \ll 1$, we can approximate the term related to the radiation field of eq 35 with its Taylor series expansion. Keeping only the linear term:

$$-1+\sqrt{\frac{1+K_W[H_2O]_{gas}}{[H_2O]_{gas}}\alpha_2\bar{\Phi}e^{a,s}+1} \cong \frac{1+K_W[H_2O]_{gas}}{[H_2O]_{gas}}\frac{\alpha_2}{2}\bar{\Phi}e^{a,s} \quad (36)$$

On the other hand, for high irradiation conditions, where $\{(1 + K_W[H_2O]_{gas}/[H_2O]_{gas}\}\alpha_2\bar{\Phi}e^{a,s} \gg 1$, the radiation field term of eq 35 can be simplified in the following way:

$$-1+\sqrt{\frac{1+K_W[H_2O]_{gas}}{[H_2O]_{gas}}\alpha_2\bar{\Phi}e^{a,s}+1} \cong \sqrt{\frac{1+K_W[H_2O]_{gas}}{[H_2O]_{gas}}\alpha_2\bar{\Phi}e^{a,s}} \quad (37)$$

This limiting behavior with respect to the irradiation level is described by Upadhya and Ollis[17] for the degradation of TCE in the gas phase.

In accord with the linear dependence of the PCE reaction rate on the irradiation level, we should consider the expression corresponding to the low irradiation limit as the one consistent with the experimental evidence. Therefore, from eqs 35 and 36:

$$r_{PCE} = -\alpha\frac{[PCE]_{gas}}{1+K_W[H_2O]_{gas}}e^{a,s} \quad (38)$$

where

$$\alpha = \frac{\alpha_1\alpha_2\bar{\Phi}}{2} = \frac{k_7K_{PCE}[Sites]\bar{\Phi}}{k_{16}[M]} \quad (39)$$

It should be noticed that the general expression proposed for the PCE degradation rate, for different values of PCE feed concentrations, relative humidity levels, and irradiation intensities, is given by eq 19. This equation should be combined with the final expression of the LSRPA (eq 33) to obtain the PCE reaction rate at each point on the catalytic plate. Equation 38 is only a simplified expression of the PCE reaction rate corresponding to the PCE−air−water vapor mixtures and the low irradiation conditions used in the experimental work.

Regression of Kinetic Parameters

The parameters in the kinetic expression (α and K_W) were regressed from experimental data using the Levenberg−Marquardt method.[25] The block diagram corresponding to the employed algorithm is shown in Figure 8a. Model values of the PCE degradation rate were calculated with eq 38 for the same operating conditions corresponding to each experimental datum obtained with eq 1. Notice that, due to the adopted photoreactor operation conditions, the PCE reaction rate was computed using the corresponding PCE concentration at the outlet stream of the loop which is the same as that in the reactor volume. To calculate eq 38, it is necessary to know the radiation absorption rate ($e^{a,s}$) as given by eqs 33 and 34. Thus, the model predictions are the result of a rather complex calculation where no adjusted parameters are needed and the experimental values of the radiation flux, measured with the radiometer, were

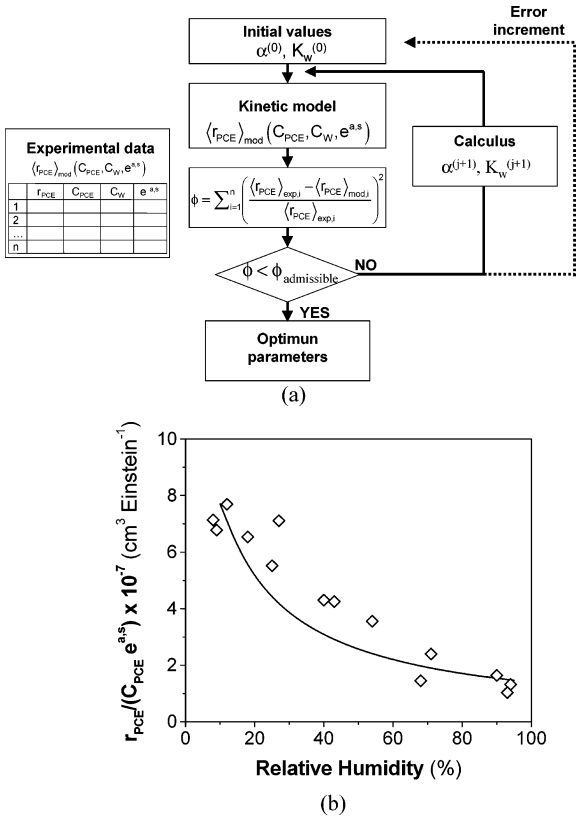

Figure 8. (a) Diagram of the employed algorithm for the parameter estimation. (b) Predicted and experimental data for different PCE concentrations and irradiation levels. Key: (◇) experimental values, (—) proposed kinetic model.

Table 3. Kinetic Parameters

parameter	value	95% confidence interval	units
α	154	19	m^3 Einstein^{-1}
K_w	5.94×10^{-4}	0.97×10^{-4}	m^3 mg^{-1}

only used to validate the proposed mathematical model for the radiation field.

The optimizing program minimized the sum of the square of the relative differences between predicted and experimental values (objective function). The results of the kinetic parameters are shown in Table 3. In Figure 8b, predicted and experimental values of the ratio $r_{PCE}/(C_{PCE}e^{a,s})$ are plotted against relative humidity. A satisfactory agreement is observed.

Conclusions

A kinetic model for PCE degradation in an air stream was developed. It shows the photocatalytic reaction rate dependence with respect to PCE concentration, the LSRPA, and humidity. It was derived from a plausible detailed mechanism.

The radiation absorption rate for the kinetic model (the LSRPA) was obtained from the results of a mathematical model that does not make use of any experimentally adjusted parameters.

The kinetic parameters were estimated from PCE reaction rate experimental data taken in a differential reactor, without mass transfer limitations, applying a nonlinear regression procedure.

The obtained results show (1) first-order kinetics with respect to PCE concentration, (2) linear dependence with respect to the irradiation level, and (3) site-competitive kinetics for the dependence on the relative humidity.

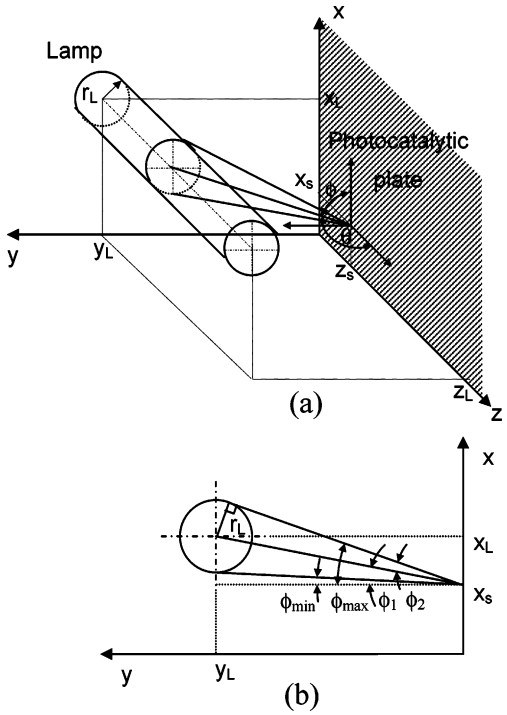

Figure 9. (a) Coordinate system for defining the limiting angles of integration in the radiation emission model. (b) Projection on an $(x-y)$ plane.

Acknowledgment

The authors are grateful to Universidad Nacional del Litoral (UNL), Consejo Nacional de Investigaciones Científicas y Técnicas (CONICET), and Agencia Nacional de Promoción Científica y Tecnológica (ANPCyT) for the financial support. Thanks are also given to Eng. Gerardo Rintoul for his participation in some parts of the experimental work.

Appendix

Integration Limits for the Three-Dimensional Superficial Emission Model. The following assumptions were made for the lamp: (1) the lamp is a perfect cylinder, (2) the photon emitters are distributed uniformly on the lamp surface, (3) each point of the lamp surface emits isotropically, and (4) there are no changes in the direction or intensity of the rays when they leave the surface of the lamp.

Figure 9a shows the coordinate system adopted: A spherical coordinate system (r,θ,ϕ) placed at a point on the photocatalytic surface that is located in a Cartesian coordinate system (x,y,z). Figure 9b shows the previous figure projected on the $(x-y)$ plane. According to that, the azimuthal limiting angles are given by:

$$\phi_{max} = \phi_1 + \phi_2 \quad \phi_{min} = \phi_1 - \phi_2 \tag{A.1}$$

Using trigonometric relationships:

$$\phi_{max} = \tan^{-1}\left(\frac{x_L - x_s}{y_L}\right) + \sin^{-1}\left(\frac{r_L}{\sqrt{(x_L - x_s)^2 + {y_L}^2}}\right) \tag{A.2}$$

$$\phi_{\min} = \tan^{-1}\left(\frac{x_L - x_s}{y_L}\right) - \sin^{-1}\left(\frac{r_L}{\sqrt{(x_L - x_s)^2 + y_L{}^2}}\right) \quad (A.3)$$

The coordinates of the points located on the surface of the lamp are given by:

$$r_L{}^2 = (y - y_L)^2 + (x - x_L)^2 \quad (A.4)$$

where x and y may be related with the azimuthal angle by:

$$\tan\phi = \frac{(x - x_s)}{y} \quad (A.5)$$

Expressing eq A.4 in terms of the azimuthal angle:

$$x(\phi) = x_L + (x_s - x_L)\cos^2\phi + y_L \cos\phi \sin\phi - \sin\phi\sqrt{r_L{}^2 - (y_L \sin\phi + (x_s - x_L)\cos\phi)^2} \quad (A.6)$$

$$y(\phi) = y_L \cos^2\phi - (x_s - x_L)\cos\phi \sin\phi - \cos\phi\sqrt{r_L{}^2 - (y_L\sin\phi + (x_s - x_L)\cos\phi)^2} \quad (A.7)$$

The polar angle may be calculated employing the following relationship: $\cos\theta = \underline{\Omega}\cdot\underline{n}_z/|\underline{\Omega}|$, and according to the chosen coordinate system $\underline{\Omega}_{\min} = (x(\phi) - x_s, y(\phi), -z_s)$, $\underline{\Omega}_{\max} = (x(\phi) - x_s, y(\phi), z_L - z_s)$, and $\underline{n}_z = (0,0,1)$. Therefore:

$$\cos\theta_{\min}(\phi) = \frac{-z_s}{\sqrt{(x(\phi) - x_s)^2 + y(\phi)^2 + z_s{}^2}} \quad (A.8)$$

$$\cos\theta_{\max}(\phi) = \frac{z_L - z_s}{\sqrt{(x(\phi) - x_s)^2 + y(\phi)^2 + (z_L - z_s)^2}} \quad (A.9)$$

Finally, substituting eqs A.6 and A.7 into eqs A.8 and A.9:

$$\cos\theta_{\min}(\phi) = \frac{-z_s}{\sqrt{z_s{}^2 + r_L{}^2 + (x_s - x_L)^2 + y_L{}^2 - 2\beta_1(\phi)^2 - 2\beta_2(\phi)\sqrt{r_L{}^2 - \beta_1(\phi)^2}}} \quad (A.10)$$

$$\cos\theta_{\max}(\phi) = \frac{z_L - z_s}{\sqrt{(z_L - z_s)^2 + r_L{}^2 + (x_s - x_L)^2 + y_L{}^2 - 2\beta_1(\phi)^2 - 2\beta_2(\phi)\sqrt{r_L{}^2 - \beta_1(\phi)^2}}} \quad (A.11)$$

where

$$\beta_1(\phi) = y_L \sin\phi + (x_s - x_L)\cos\phi \quad (A.12)$$

$$\beta_2(\phi) = -y_L \cos\phi + (x_s - x_L)\sin\phi \quad (A.13)$$

Nomenclature

Ar = reaction area of the photocatalytic plate, cm^2
C = concentration, mg m^{-3}
e = thickness, cm
$e^{a,s}$ = local superficial rate of photon absorption, Einstein s^{-1} cm^{-2}
I = specific radiation intensity, Einstein s^{-1} cm^{-2} sr^{-1}
K = equilibrium constant, m^3 mg^{-1}
k_i = kinetic constant of the i reaction, units depend on the reaction step
$\underline{n}_G$ = unit outwardly directed normal to the catalytic film, dimensionless
P = emission power, W
Q = volumetric flow rate, cm^3 s^{-1}
q = local net radiation flux, Einstein s^{-1} cm^{-2}
$\underline{q}$ = local radiation flux vector, Einstein s^{-1} cm^{-2}
r = reaction rate, mol cm^{-2} s^{-1}
r_L = lamp radius, cm
$\underline{x}$ = position vector, cm
x = x coordinate, cm
y = y coordinate, cm
z = z coordinate, cm

Greek Letters

α = kinetic parameter, m^3 Einstein^{-1}
β_1,β_2 = variables defined in eqs (A.12) and (A.13)
ϕ = spherical coordinate, rad
Φ = primary quantum yield, mole Einstein^{-1}
κ = volumetric absorption coefficient, cm^{-1}
λ = wavelength, nm
θ = spherical coordinate, rad
Ω = solid angle, sr

Subscripts

λ = wavelength
a = relative to acrylic
ads = adsorption
Ar = reaction area of the photocatalytic plate
dir = direct net radiative flux
e^- = relative to the semiconductor valence band electron
f = relative to the TiO_2 film
g = relative to the electron−hole generation step; also relative to glass
gas = gaseous phase
h^+ = relative to semiconductor valence band hole
ind = indirect net radiative flux
L = relative to the UV lamp
max = relative to the maximum limit value
min = relative to the minimum limit value
n = normal to the reaction area of the photocatalytic plate
$OH^\bullet$ = relative to hydroxyl radical
PCE = relative to perchloroethylene
W = relative to water

Superscripts

i = related to the incident radiation flux
in = relative to the inlet stream of the recycle
out = relative to the outlet stream of the recycle
t = related to the transmitted radiation flux

Special Symbols

$[\cdot]$ = concentration of specific species
$\bar{\cdot}$ = averaged value over the wavelength interval
$\langle\cdot\rangle$ = average value over a defined space

Literature Cited

(1) Al-Ekabi, H.; Butters, B.; Delany, D.; Holden, W.; Powell, T.; Story, J. The Photocatalytic Destruction of Gaseous Trichloroethylene and Tetrachloroethylene Over Immobilized Titanium Dioxide. In *Photocatalytic Purification and Treatment of Water and Air*; Ollis, D. F., Al-Ekabi, H., Eds.; Elsevier: Amsterdam/New York, 1993; pp 719−725.

(2) Fukami, N.; Yosida, M.; Lee, B. D.; Taku, K.; Hosomi, M. Photocatalytic Degradation of Gaseous Perchloroethylene: Products and Pathway. *Chemosphere* **2001**, *42*, 345.

(3) Yamazaki, S.; Tsukamoto, H.; Araki, K.; Tanimura, T.; Tejedor-Tejedor, I.; Anderson, M. A. Photocatalytic Degradation of Gaseous Tetrachloroethylene on Porous TiO_2 Pellets. *Appl. Catal., B* **2001**, *33*, 109.

(4) Yamazaki, S.; Araki, K. Photocatalytic Degradation of Tri- and Tetrachloroethylene on Porous TiO_2 Pellets. *Electrochemistry* **2002**, *70*, 412.

(5) Anderson, M. A.; Yamazaki-Nishida, S.; Cervera-March, S. Photodegradation of Trichloroethylene in the Gas Phase Using TiO_2 Porous Ceramic Membrane. In *Photocatalytic Purification and Treatment of Water and Air*; Ollis, D. F., Al-Ekabi, H., Eds.; Elsevier: Amsterdam/New York, 1993; pp 405−420.

(6) Luo, Y.; Ollis, D. F. Heterogeneous Photocatalytic Oxidation of Trichloroethylene and Toluene Mixtures in Air: Kinetic Promotion and Inhibition, Time-Dependent Catalyst Activity. *J. Catal.* **1996**, *163*, 1.

(7) Kim, J. S.; Itoh, K.; Murabayashi, M.; Kim, B. A. Pretreatment of the Photocatalyst and the Photocatalytic Degradation of Trichloroethylene in the Gas-Phase. *Chemosphere* **1999**, *38*, 2969.

(8) Li, G. H.; An, W. Z. A Proposed Mechanism of Photocatalytic Oxidation of Trichloroethylene in Gas Phase. *Chin. Chem. Lett.* **2000**, *11*, 31.

(9) Zhao, L.; Ozaki, S.; Itoh, K.; Murabayashi, M. Self-Catalytic Behavior in Gas-Phase Photocatalytic Oxidation of Trichloroethylene Using TiO_2. *Electrochemistry* **2002**, *70*, 8.

(10) Wang, K. H.; Jehng, J. M.; Hsieh, Y. H.; Chang, C. Y. The Reaction Pathway for the Heterogeneous Photocatalysis of Trichloroethylene in Gas Phase. *J. Hazard. Mater*. **2002**, *B90*, 63.

(11) Dibble, L. A.; Raupp, G. B. Kinetics of the Gas-Solid Heterogeneous Photocatalytic Oxidation of Trichloroethylene by Near UV Illuminated Titanium Dioxide. *Catal. Lett*. **1990**, *4*, 345.

(12) Hung, C. H.; Mariñas B. J. Role of Water in the Photocatalytic Degradation of Trichloroethylene Vapor on TiO_2 Films. *Environ. Sci. Technol*. **1997**, *31*, 1440.

(13) Amama, P. B.; Itoh, K.; Murabayashi, M. Photocatalytic Oxidation of Trichloroethylene in Humidified Atmosphere. *J. Mol. Catal. A: Chem.* **2001**, *176*, 165.

(14) Wang, K. H.; Tsai, H. H.; Hsieh, Y. H. The Kinetics of Photocatalytic Degradation of Trichloroethylene in Gas Phase over TiO_2 Supported on Glass Bead. *Appl. Catal., B* **1998**, *17*, 313.

(15) Kim, S. B.; Hong, S. C. Kinetic Study for Photocatalytic Degradation of Volatile Compounds in Air Using Thin Film TiO_2 Photocatalyst. *Appl. Catal., B* **2002**, *35*, 305.

(16) Yamazaki-Nishida, S.; Nagano, K. J.; Phillips, L. A.; Cervera-March, S.; Anderson, M. A. Photocatalytic Degradation of Trichloroethylene in the Gas Phase Using Titanium Dioxide Pellets. *J. Photochem. Photobiol., A* **1993**, *70*, 95.

(17) Upadhya, S.; Ollis, D. F. A Simple Kinetic Model for the Simultaneous Concentration and Intensity Dependencies of TCE Photocatalyzed Destruction. *J. Adv. Oxid. Technol.* **1998**, *3*, 199.

(18) Cassano, A. E.; Martín, C. A.; Brandi, R. J.; Alfano, O. M. Photoreactor Analysis and Design: Fundamentals and Applications. *Ind. Eng. Chem. Res.* **1995**, *34*, 2155.

(19) Esterkin, C. R.; Negro, A. C.; Alfano, O. M.; Cassano, A. E. Air Pollution Remediation in a Fixed Bed Photocatalytic Reactor Coated with TiO_2. *AIChE J.*, in press.

(20) Jackson, N. B.; Wang, C. M.; Luo, Z.; Schwitzgebel, J.; Eckerdt, J. G.; Brock, J. R.; Heller, A. Attachment of TiO_2 Powders to Hollow Glass Microbeads: Activity of the TiO_2-Coated Beads in Photoassisted Oxidation of Ethanol to Acetaldehyde. *J. Electrochem. Soc.* **1991**, *138*, 3660.

(21) Sanhueza, E.; Hisatsune, I. C.; Heiklen, J. Oxidation of Haloethylenes. *Chem. Rev.* **1976**, *76*, 801.

(22) Hung, C. H.; Mariñas, B. J. Role of Chlorine and Oxygen in the Photocatalytic Degradation of Trichloroethylene Vapor on TiO_2 Films. *Environ. Sci. Technol*. **1997**, *31*, 562.

(23) Sauer, M. L.; Hale, M. A.; Ollis, D. F. Heterogeneous Photocatalytic Oxidation of Dilute Toluene-Chlorocarbon Mixtures in Air. *J. Photochem. Photobiol., A* **1995**, *88*, 169.

(24) Siegel, R.; Howell, J. R. *Thermal Radiation Heat Transfer*, 3rd ed.; Hemisphere: Washington, DC, 1992.

(25) Press, W. H.; Teukolsky, S. A.; Vetterling, W. T.; Flannery, B. P. *Numerical Recipes*, 2nd ed.; Cambridge University Press: New York, 1996.

Received for review August 31, 2004
Revised manuscript received December 18, 2004
Accepted December 29, 2004

IE049185Z